metals

MDPI

Article

Revisiting Rare Earth Permanent Magnetic Alloys of Nd-Fe-C

Jianing Fan, Bang Zhou, Hongya Yu and Zhongwu Liu *

School of Materials Science and Engineering, South China University of Technology, Guangzhou 510640, China; 202220120358@mail.scut.edu.cn (J.F.); 18846321367@163.com (B.Z.); yuhongya@scut.edu.cn (H.Y.)
* Correspondence: zwliu@scut.edu.cn; Tel.: +86-159-2089-5122

Abstract: Nd-Fe-C alloys have been reported as hard magnetic materials with a potential higher coercivity than Nd-Fe-B alloys. However, it has been seldom studied since its intrinsic properties were investigated in the last century. Here, we revisited the structure, phase precipitation and magnetic properties of rapidly quenched ternary Nd-Fe-C alloys for further understanding their composition-microstructure-property relationships. The $Nd_{10+x}Fe_{84-x}C_6$ (x = −2, 0, 2, 3, 4, 5) alloys with various compositions were prepared by melt spinning. The results show that the hard magnetic $Nd_2Fe_{14}C$ phase can be hardly formed in the as-spun alloys. Instead, the alloys are composed of soft magnetic α-Fe phase and planar anisotropic $Nd_2Fe_{17}C_x$ phase. After annealing above 650 °C, the $Nd_2Fe_{14}C$ phase is precipitated by the peritectoid reaction. All optimally annealed alloys contain $Nd_2Fe_{14}C$ and $Nd_2Fe_{17}C_x$ phases, while the presence and content of α-Fe phase are determined by the alloy composition. The crystallization degree of the as-spun alloys has an effect on their magnetic properties after annealing. After the annealing treatment, partly crystallized as-spun alloys exhibit better magnetic properties than the amorphous alloys. The intrinsic coercivity H_{cj} = 847 kA/m, remanence J_r = 0.69 T, and maximum energy product $(BH)_{max}$ = 64.3 kJ/m^3 were obtained in the $Nd_{14}Fe_{80}C_6$ alloy annealed at 725 °C. The formation of the $Nd_2Fe_{14}C$ and $Nd_2Fe_{17}C_x$ phases with the Nd_2O_3 phase precipitated at the triangular grain boundaries is responsible for its relatively good properties. Although the magnetic properties of Nd-Fe-C alloys obtained in this work are inferior to those of Nd-Fe-B, the present results help us to further understand the magnetic behavior of Nd-Fe-C alloys.

Keywords: Nd-Fe-C alloys; permanent magnet; melt spinning; phase precipitation; magnetic properties

Citation: Fan, J.; Zhou, B.; Yu, H.; Liu, Z. Revisiting Rare Earth Permanent Magnetic Alloys of Nd-Fe-C. *Metals* **2024**, *14*, 1115. https://doi.org/10.3390/met14101115

Received: 1 September 2024
Revised: 25 September 2024
Accepted: 27 September 2024
Published: 30 September 2024

1. Introduction

Since the discovery in the early 1980s, Nd-Fe-B magnets have emerged as the strongest permanent magnets available, attributed to the exceptional magnetic properties inherent in the $Nd_2Fe_{14}B$ compound. This compound boasts both high saturation magnetization M_s and a remarkable anisotropy field H_A, making it an ideal candidate for achieving unparalleled magnetic strength [1]. In fact, shortly after the invention of $Nd_2Fe_{14}B$, the $Nd_2Fe_{14}C$ compound was also found to have a similar structure as $Nd_2Fe_{14}B$ by neutron diffraction [2]. Although the Curie temperature T_C = 535 K [3] and the saturation magnetization M_s = 1.4 T of $Nd_2Fe_{14}C$ are slightly lower than those of $Nd_2Fe_{14}B$, its higher H_A of about 10 T is a significant advantage [4]. Thus, Nd-Fe-C alloys were considered to have potential as working alternatives of Nd-Fe-B with a high coercivity and energy product.

However, the investigation on Nd-Fe-C magnets remains very limited. Although some earlier studies gave the structure and intrinsic properties of the $Nd_2Fe_{14}C$ compounds, researchers have struggled to achieve high extrinsic properties in these alloys. In 1987, Buschow et al. [5] showed that the as-cast Nd-Fe-C alloys need to be annealed in a narrow range of 830–890 °C for about 500 h to obtain the $Nd_2Fe_{14}C$ phase. A lower annealing temperature leads to low reaction kinetics, while a higher temperature will cause the transformation of $Nd_2Fe_{14}C$ to $Nd_2Fe_{17}C_X$. Then in 1988, De Mooij and Buschow [3] reported that this $Nd_2Fe_{17}C_x$ compound has a rhombohedral structure and that the carbon

atom occupies a separate lattice position. And its Curie temperature T_C increases with increasing x [3,6]. In the same year, Denissen et al. [7] reported that a spin reorientation occurred for $Nd_2Fe_{14}C$ at about 140 K, which is the same temperature for $Nd_2Fe_{14}B$. In 1989, Coehoorn [4] found that $Nd_2Fe_{14}C$ can be obtained by melt spinning followed by a short-time anneal treatment because the phase transformation in as-spun alloys is faster than in the casting alloys. After annealing at 730 °C, $Nd_{13.5}Fe_{79.6}C_{6.9}$ ribbons prepared at the wheel speed of 28 m/s exhibit H_{cj} = 797.1 kA/m and J_r = 0.72 T. In 1990 and 1991, Grieb et al. [8,9] reported the phase diagram of a ternary Nd-Fe-C alloy, which shows that the $Nd_2Fe_{14}C$ phase is precipitated from Nd_2Fe_{17}, α-Fe and corrosive Nd-carbides phases by a peritectoid reaction below 890 °C. In 1994, Fernengel [10] prepared sintered Nd-Fe-C alloys through a conventional powder metallurgy process. The sintered magnet was almost isotropic and exhibited a low coercivity of about 250 kA/m. In a study conducted from 1996 to 1998, Sui et al. [11–13] concluded that the $Nd_2Fe_{14}C$ phase can also be formed by mechanical alloying and subsequent annealing. After annealing at 900 °C, $Nd_{16}Fe_{75.8}C_{8.2}$, which contains the $Nd_2Fe_{17}C_x$ phase, exhibits the optimal coercivity H_{cj} = 597.1 kA/m.

In the 21st century, research on the Nd-Fe-C magnets is still not very popular. A few studies focused on the improvement of magnetic properties by different preparation methods and adding different elements, including B [14,15], Dy [16,17], Cu [18] and Co [19,20]. For example, Geng et al. [15] achieved relatively good magnetic properties with J_r = 0.73 T, H_{cj} = 1193.7 kA/m and $(BH)_{max}$ = 91.7 kJ/m^3 by high-energy ball-milling the $Nd_2Fe_{11}B_{0.06}$ alloy in heptane (C_7H_{16}), followed by annealing. Although a B substitution for C can optimize the magnetic properties of Nd-Fe-C alloy, it actually leads to the Nd-Fe-B system.

Until now, the high intrinsic properties of $Nd_2Fe_{14}C$ compound has not given good magnetic properties for Nd-Fe-C alloys. In particular, high H_A has not been reflected by a high coercivity. As we know, currently, the coercivity of Nd-Fe-B magnets is still not high enough for some applications at a relatively high temperature. The coercivity enhancement of Nd-Fe-B magnets generally relies on the resource-constrained heavy rare earth (HRE) elements of Dy and Tb [21,22], which leads to the high material cost. Therefore, looking for low-cost new compounds with a higher H_A is urgently needed for developing high coercive magnets. In this sense, exploring Nd-Fe-C alloys with high coercivity is extremely meaningful. In this work, aiming at understanding the phase evolution, microstructures and magnetic properties of Nd-Fe-C system, we revisit the ternary Nd-Fe-C alloys prepared by melt spinning and heat treatment. Our work is expected to revitalize the research on Nd-Fe-C permanent magnets for finding high coercivity magnets with less use of HRE elements.

2. Materials and Methods

The alloy ingots with nominal compositions of $Nd_{10+x}Fe_{84-x}C_6$ (x = 0, 2, 3, 4, 5) were prepared by arc-melting under an argon atmosphere using Nd, Fe and C bulks with a purity greater than 99.9% as raw materials. Each ingot was re-melted five times to ensure compositional homogeneity. Melt-spun amorphous and nanocrystalline ribbons were obtained by quenching the molten metal on the copper wheel at linear speeds of 10–50 m/s. Parts of ribbons were annealed at different temperatures for 10 min after being sealed in a quartz tube with argon as the protecting gas. The phase identification was characterized by the X-ray diffraction (XRD, X' Pert Pro, PANalytical, Almelo, Netherlands) with Cu Kα radiation. The crystallization and phase precipitation temperatures were investigated by a differential scanning calorimeter (DSC, Netzsch 404 F3, Selb, Germany) under a flowing argon atmosphere. The magnetic properties of alloys were measured by a vibrating sample magnetometer (VSM) in the physical properties measurement system (PPMS-9, Quantum Design, San Diego, California, CA, USA). The magnetization–temperature curves were measured at a magnetic field H = 1000 Oe in the temperature range of 300–800 K. The microstructure of the selected sample was observed using transmission electron microscopy (TEM, FEI Talos F200×, Hillsboro, Oregon, OR, USA).

3. Results

3.1. Phase Constitution and Magnetic Properties of Directly Quenched $Nd_{12}Fe_{82}C_6$ Alloy

Figure 1a shows the XRD patterns of $Nd_{12}Fe_{82}C_6$ alloys prepared at the wheel speeds of 10–50 m/s. The as-quenched alloys contain the $Nd_2Fe_{17}Cx$ phase (i.e., 2:17 phase) and the α-Fe phase, while the $Nd_2Fe_{14}C$ phase (i.e., 2:14:1 phase) is not detected. For the alloy obtained at 10 m/s, the peak intensities of α-Fe phase are comparable to those of the 2:17 phase. As the wheel speed increases over 20 m/s, the peaks of the α-Fe phase become weak. When the speed reaches 30 m/s or more, the peaks become broader, indicating the refinement of the grains or the appearance of the amorphous phase. For the alloy prepared at 50 m/s, the crystallization peaks are almost invisible and the amorphous phase is dominated.

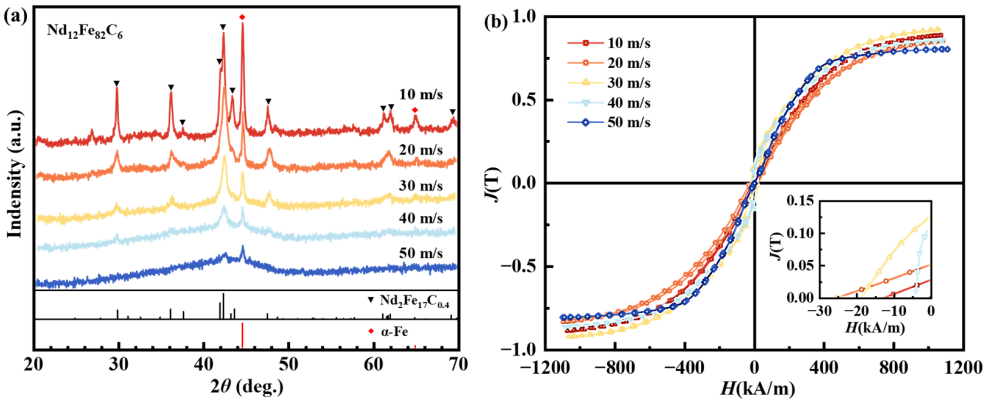

Figure 1. (**a**) XRD patterns and (**b**) magnetic hysteresis loops of melt-spun $Nd_{12}Fe_{82}C_6$ alloys prepared at various wheel speeds.

Figure 1b presents the magnetic hysteresis curves of as-quenched $Nd_{12}Fe_{82}C_6$ alloys. The horizontal axis of the magnetic hysteresis curves represents the magnetic field intensity *H*, while the vertical axis corresponds to the magnetic polarization intensity *J*. All alloys show low coercivity, since both α-Fe and Nd_2Fe_{17} phase are soft magnetic [19]. The magnetic properties of this alloy are influenced by the contents of 2:17, α-Fe and amorphous phases obtained at different wheel speeds. The alloy prepared at 20 m/s exhibits a moderate coercivity of 28 kA/m, which is attributed more to the 2:17 phase with planar anisotropy. Hence, the above results indicate that the $Nd_2Fe_{14}C$ phase cannot be formed directly during rapid solidification of the liquid Nd-Fe-C alloy, resulting in a low coercivity of as-spun alloys.

3.2. Phase Precipitation Behavior and Magnetic Properties of Annealed $Nd_{12}Fe_{82}C_6$ Alloy

Figure 2a shows the DSC curve of the amorphous $Nd_{12}Fe_{82}C_6$ alloy prepared at the wheel speed of 50 m/s. Two exothermic peaks are observed at 607.8 °C and 660.6 °C. The endothermic peak appearing at 893.6 °C can be attributed to the decomposition temperature of 2:14:1 phase based on the Nd-Fe-C ternary phase diagram [9]. In order to understand the phase precipitation behavior of the alloy during heating, the amorphous $Nd_{12}Fe_{82}C_6$ alloy was annealed at temperatures between 550 °C and 950 °C for 10 min, and the XRD patterns are shown in Figure 2b. After annealing at 550 °C, the diffraction peaks of the alloy exhibit distinct amorphous characteristics, indicating the retention of the original amorphous state. Upon increasing the temperature to 600 °C, the amorphous phase starts to crystallize, accompanied by the precipitation of α-Fe and 2:17 phases. The peak intensities of the 2:14:1 phase gradually increase with the increasing temperature. After annealing at 700 °C, a notable enhancement of the peak intensity for 2:14:1 phase is obtained. As the temperature further increases, the peak intensity of α-Fe decreases significantly, and more of the 2:14:1 phase is formed. Based on the XRD results and phase diagram [9], the phase transitions at 607.8 °C and 660.6 °C shown on the DSC curve can be identified as the crystallization of amorphous phase and the precipitation of 2:14:1 phase, respectively.

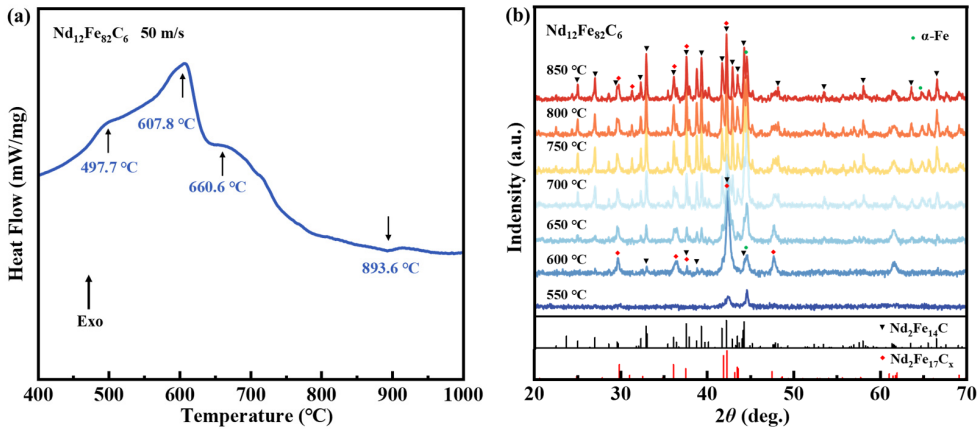

Figure 2. (**a**) DSC curve for the amorphous $Nd_{12}Fe_{82}C_6$ alloy and (**b**) XRD patterns for the amorphous $Nd_{12}Fe_{80}C_6$ alloy annealed at various temperatures.

Figure 3a,b shows the 2nd quadrant demagnetization curves and magnetic properties of $Nd_{12}Fe_{82}C_6$ alloys annealed at various temperatures, respectively. With the increase in annealing temperature from 750 °C to 875 °C, the intrinsic coercivity H_{cj} and the maximum energy product $(BH)_{max}$ showed a tendency to increase, and the remanence J_r slightly increased. This phenomenon is primarily attributed to an enhanced precipitation of the hard magnetic 2:14:1 phase, coupled with a concurrent decrease in the contents of both the 2:17 and α-Fe phases. After annealing at 875 °C for 10 min, the best hard magnetic properties with J_r = 0.60 T, H_{cj} = 425 kA/m and $(BH)_{max}$ = 35 kJ/m^3 were obtained. After annealing at 900 °C, the magnetic properties decreased, which resulted from the decomposition of 2:14:1 phase [3] and the abnormal 2:17 grains growth [18]. The remanence enhancement effect, manifested by a J_r/J_s ratio greater than 0.5, was also observed in these annealed alloys. The exchange coupling between these soft magnetic phases (α-Fe and 2:17 phases) and the hard magnetic $Nd_2Fe_{14}C$ phase at the nanoscale enhances the transfer of magnetic moments. As a result, when an external magnetic field was applied and then removed, a higher proportion of the magnetization was retained, leading to the observed increase in the residual magnetization (J_r) relative to the saturation magnetization (J_s), resulting in $J_r/J_s > 0.5$. However, for all annealed alloys, the demagnetization curves show low squareness and a clear collapsed shoulder shape, indicating a poor exchange coupling between the grains [23]. In conclusion, for the amorphous $Nd_{12}Fe_{82}C_6$ alloy, the optimum annealing temperature is near 875 °C. The magnetic properties of the alloy are not satisfactory due to the presence of the 2:17 and α-Fe phases.

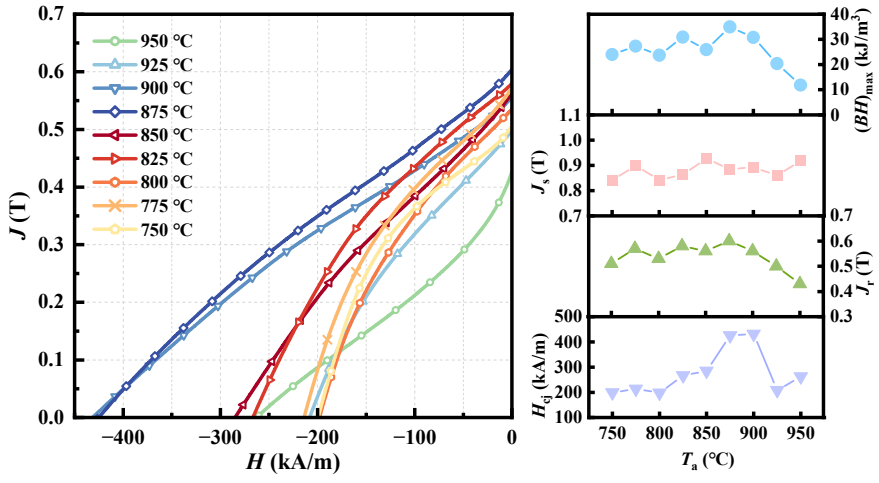

Figure 3. (**a**) Demagnetization curves and (**b**) hard magnetic properties of $Nd_{12}Fe_{82}C_6$ alloys annealed at various temperatures.

3.3. Effects of Nd Content on the Annealed Nd-Fe-C Alloys

Based on the phase diagram of the Nd-Fe-C ternary alloy, significant variations in the phase composition were observed among alloys with differing Nd contents [9]. The $Nd_{10+x}Fe_{84-x}C_6$ (x = −2, 0, 2, 3, 4, 5) alloys were prepared at the wheel speed of 50 m/s and annealed at various temperatures subsequently. The XRD patterns of the alloys annealed at optimum temperatures are given in Figure 4a. Both the 2:14:1 phase and the 2:17 phase were detected in all alloys and their contents were varied for different Nd contents. The diffraction peaks of α-Fe phase in the Nd-lean alloy (x = 0) were significantly stronger than those of other two compositions, indicating less of the 2:14:1 and 2:17 phase. More of the 2:17 phase and less of the α-Fe phase can be found in the x = 2 alloy. In the Nd-rich alloy (x = 3), there was no α-Fe detected. Figure 4b shows the demagnetization curves of amorphous $Nd_{10+x}Fe_{84-x}C_6$ alloys (x = −2, 0, 2, 3, 4, and 5) annealed at 875 °C. The $Nd_8Fe_{86}C_6$ and $Nd_{10}Fe_{84}C_6$ alloys exhibited very low coercivity. The coercivity for the alloys with x > 2 was greatly improved, and the squareness of the demagnetization curve was also improved. The annealed $Nd_{14}Fe_{80}C_6$ alloy shows the good curve squareness and relatively high magnetic properties with J_r = 0.58 T, H_{cj} = 542 kA/m and $(BH)_{max}$ = 45 kJ/m^3. For the alloys with excessive Nd content (x = 5), the magnetic properties decreased. The XRD results show that the α-Fe content rises in the alloy with x = 5. Therefore, the remanence of the alloy increased slightly and the coercivity decreased. The above results indicate that for the annealed Nd-Fe-C alloys, an optimized Nd content can suppress the precipitation of the α-Fe phase and improve the magnetic properties.

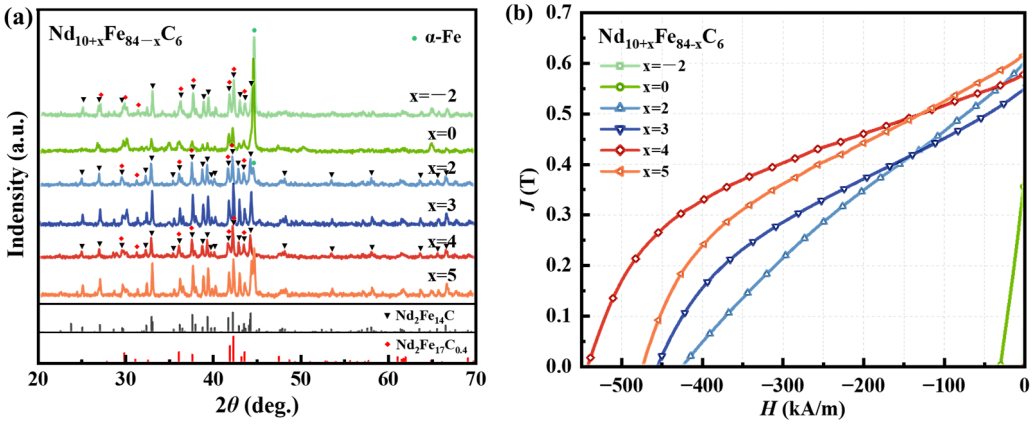

Figure 4. (**a**) XRD patterns and (**b**) demagnetization curves of amorphous $Nd_{10+x}Fe_{80-x}C_6$ (x = −2, 0, 2, 3, 4, 5) alloys annealed at 875 °C.

3.4. Optimizing the Structure and Magnetic Properties of $Nd_{14}Fe_{80}C_6$ Alloy

$Nd_{14}Fe_{80}C_6$ alloy was further optimized for high permanent magnetic properties. The effects of the crystallization state of as-spun alloys on the phase precipitation and magnetic properties of annealed alloys are investigated here. The as-spun alloys were prepared at the wheel speeds of 18, 20 and 22 m/s. The DSC curves in Figure 5a show that all alloys have two exothermic peaks at similar temperatures near 660 °C and 690 °C, which correspond to the different stages of crystallization or phase transformation. The exothermic peak near 890 °C is also an indication of the decomposition of the 2:14:1 phase. The XRD patterns for the alloys obtained at various wheel speeds and annealed at various temperatures are shown in Figure 5b–d. All as-spun alloys contain the 2:17 phase and the α-Fe phase. The broadening diffraction peaks imply that some amorphous phases may also exist in the alloys. For the alloys prepared at 18 m/s, the peak broadening disappears when the annealing temperature reaches 625 °C, while for the alloys prepared at 20 m/s and 22 m/s, the crystallization temperature is 675 °C. Combined with DSC results, the amorphous phase crystallizes at 659.0 °C, 661.0 °C and 592.9 °C for these three alloys. After annealing at 725 °C, the 2:14:1 phase precipitates in large quantities. This precipitation

process corresponds to the exothermic peaks at 696.8 °C, 693.8 °C and 691.6 °C on the DSC curves. After annealing at 775 °C, the three alloys have the same phase constitution of the 2:14:1 and 2:17 phases, and none of them contains the α-Fe phase.

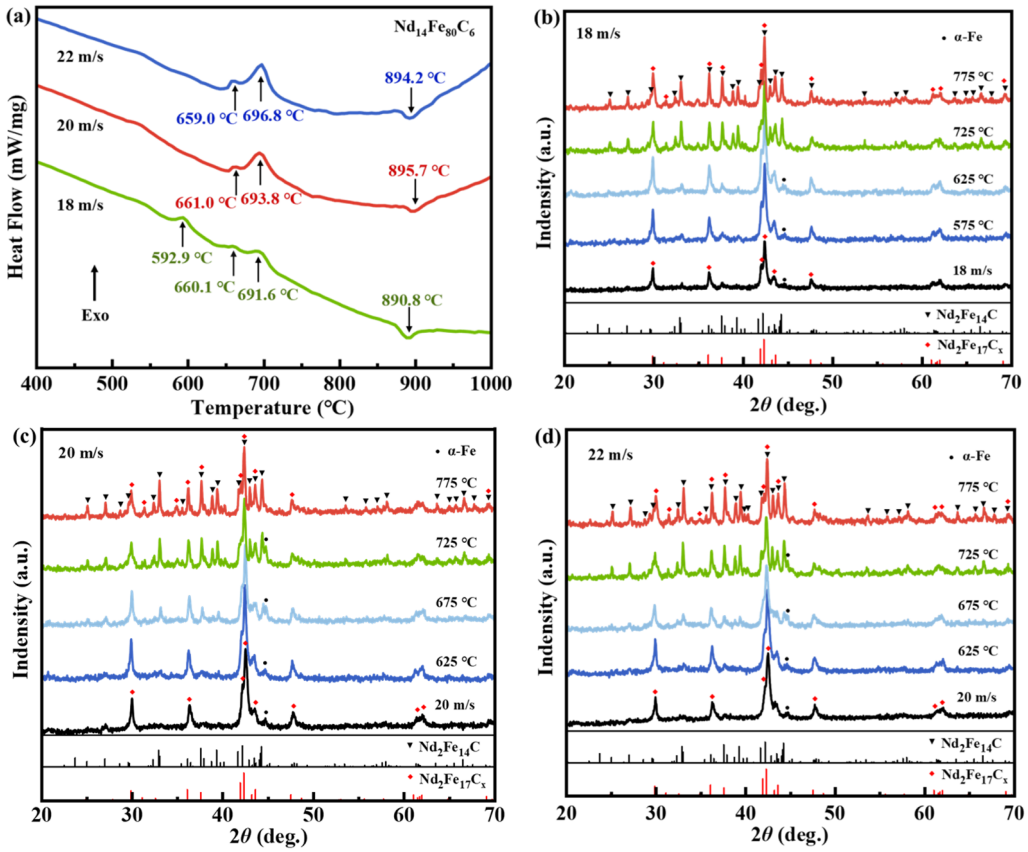

Figure 5. (**a**) DSC curves for the $Nd_{14}Fe_{80}C_6$ alloys prepared at 18, 20 and 22 m/s. XRD patterns for as-spun $Nd_{14}Fe_{80}C_6$ alloys prepared at wheel speeds of 18 m/s (**b**), 20 m/s (**c**) and 22 m/s (**d**) annealed at various temperatures.

Figure 6a–c shows magnetic hysteresis loops of the annealed alloys. It is indicated that the hard magnetic properties of all alloys increase with the increasing annealing temperature up to 775 °C due to the increasing precipitation of the 2:14:1 phase. As the contents of α-Fe and 2:17 phases reduce with the increasing of annealing temperatures, the coercivity of the alloys increases and the squareness of the demagnetization curve is improved significantly. However, the demagnetization curves still have a collapsed shoulder, indicating that these two phases are not exchange coupled. The inconsistency of the magnetization reversal of these two types of grains during demagnetization and the possible structural inhomogeneities leads to the collapsed shoulder shape of the hysteresis loops [20]. Figure 6d shows the hysteresis loops of the as-spun alloys prepared at 18, 20 and 22 m/s after annealing at their respective optimal temperatures. The partly crystallized $Nd_{14}Fe_{80}C_6$ alloy prepared at 20 m/s and subsequently annealed at 725 °C exhibits optimal magnetic properties with J_r = 0.70 T, H_{cj} = 847 kA/m and $(BH)_{max}$ = 64 kJ/m^3 in this work. The above results indicate that compared to amorphous alloys, partially crystallized alloys are capable of achieving superior permanent magnetic properties at lower annealing temperatures.

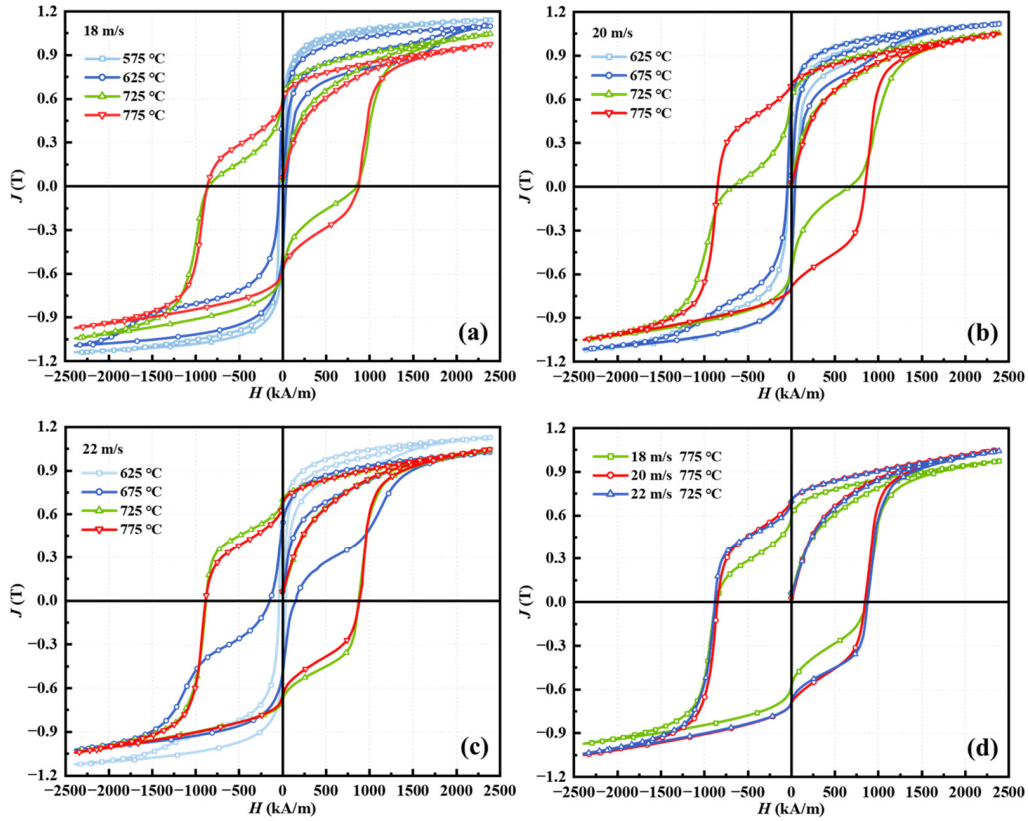

Figure 6. Hysteresis loops for $Nd_{14}Fe_{80}C_6$ alloys prepared at (**a**) 18, (**b**) 20 and (**c**) 22 m/s and annealed at different temperatures, and (**d**) the hysteresis loops for the annealed alloys obtained at optimum annealing treatment.

3.5. Microstructure of Annealed $Nd_{14}Fe_{80}C_6$ Alloy

Figure 7a,b shows the dark-field transmission electron microscopy (TEM) images for the $Nd_{14}Fe_{80}C_6$ alloy prepared at the wheel speed of 20 m/s and subsequently annealed at 775 °C. The grain sizes observed in Figure 7a varies from dozens to hundreds of nanometers. By treating all grains in Figure 7a as equiaxed crystals and measuring their perimeter, the approximate diameters of all grains were calculated. The grain size shows a normal distribution with a mean size of 138.6 nm, as shown in Figure 7c. However, the size distribution is not uniform and the grain size varies from 40.4 nm to 342.3 nm.

The high-resolution transmission electron microscopy (HRTEM) images of the selected grains 1, 2 and 3 in Figure 7b are shown in Figures 7d, 7e and 7f, respectively. The corresponding fast Fourier transformation (FFT) patterns and the interplanar distances in Figure 7d,e insets correspond well to the 2:14:1 phase and the 2:17 phase, respectively. In addition, the diffraction patterns in Figure 7f inset indicate that Grain 3 in Figure 7b belongs to the Nd_2O_3 phase.

The distribution of Nd, Fe, C and O elements for Figure 7b is shown in Figure 7g. The region with high Nd and O contents is identified as the Nd_2O_3 phase. These small Nd_2O_3 grains are distributed at quadrilateral and triangular grain boundaries. The C element is also significantly enriched in the region where the Nd_2O_3 phase is located. In addition, it is easy to distinguish the other two phases by the distribution of Nd and Fe elements. The ratio of Nd/Fe is 14.3% for the 2:14:1 phase, while it is 11.7% for the 2:17 phase. Thus, the grains with less Nd and more Fe are the 2:17 phase. From Figure 7a,b, the 2:14:1 phase is dominant and exhibits relatively large grain sizes. The 2:17 phase is randomly distributed with grain sizes between those of 2:14:1 and Nd_2O_3 phase. Figure 7h,i shows energy-dispersive X-ray spectroscopy (EDS) line scanning along *Line 1* and *Line 2* in Figure 7b. The results confirm that these three types of grains are directly connected with each other and do not exhibit any additional compositional variation related to intergranular phases. In summary, the

annealed $Nd_{14}Fe_{80}C_6$ alloy exhibits a coexistence of 2:14:1, 2:17 and Nd_2O_3 phases. These phases are randomly distributed with varied grain sizes and in direct contact with each other. Such an undesirable microstructure adversely affects the magnetic properties of the alloys.

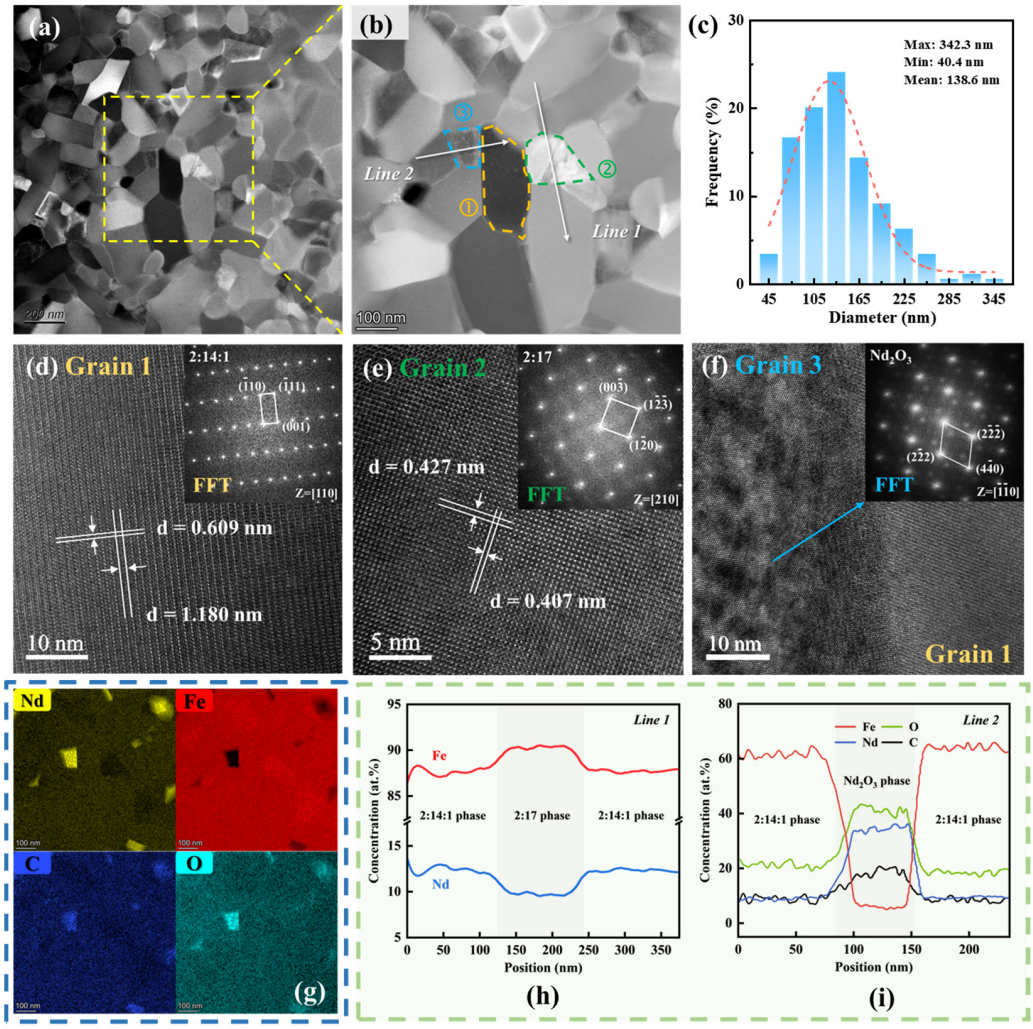

Figure 7. (**a**,**b**) Dark field TEM images and (**c**) grain size distribution for the $Nd_{14}Fe_{80}C_6$ alloy prepared at the wheel speed of 20 m/s and annealed at 775 °C. (**d**–**f**) The HRTEM images of selected grains in (**b**) and the corresponding FFT plots shown in the insets. (**g**) EDS mapping and (**h**,**i**) EDS line scanning results obtained from (**b**).

4. Discussion

Based on the above results, the Nd-Fe-C system shows distinct behaviors from Nd-Fe-B in Figure 7. According to the relevant phase diagrams for the Nd-Fe-B system and the Nd-Fe-C system [9,24], the hard magnetic $Nd_2Fe_{14}X$ (X = B, C) phases can be precipitated in both systems. In the Nd-Fe-B system, the $Nd_2Fe_{14}B$ phase is precipitated from liquid and the γ-Fe phases by a peritectic reaction at about 1180 °C. In contrast, the phase transition process in Nd-Fe-C alloys is much more complicated. The phase region of $Nd_2Fe_{14}C$ is not adjacent to the liquid phase, which explains that $Nd_2Fe_{14}C$ cannot be directly obtained by melt spinning in Nd-Fe-C alloys. $Nd_2Fe_{14}C$ must be formed by a peritectoid reaction at 600–890 °C. In addition, the phase composition of the alloys is sensitive to the Nd content. The composition region in which the $Nd_2Fe_{14}C$ is formed is narrow. Thus, the Nd_2Fe_{17}, α-Fe, Nd-carbide, and some uncertain phases may coexist with the hard magnetic phase for different compositions.

In this work, the as-spun alloys detected by XRD mainly consist of the planar anisotropic 2:17 phase and the soft magnetic α-Fe phase, leading to a low H_{cj} and J_r shown in Figure 1b. After annealing the alloy at a relatively high temperature, the 2:17 and α-Fe phases undergo a peritectoid reaction to form 2:14:1 phase. Those phases generally remained in the annealed alloys. As shown in Figure 4a, the residue of the second phase is related to the composition of alloys. The α-Fe phase content in the annealed $Nd_{10}Fe_{80}C_6$ alloy is significantly higher than those in the $Nd_{12}Fe_{82}C_6$ and $Nd_{14}Fe_{80}C_6$ alloys. The reason could be that there is not enough Nd in the $Nd_{10}Fe_{80}C_6$ alloy to form a 2:17 phase and thus more α-Fe phase is left. The lack of a 2:17 phase in the peritectoid reaction also leads to a decreased content in the 2:14:1 phase. Thus, the alloy has poor magnetic properties. For the same reason, the $Nd_{14}Fe_{80}C_6$ alloy contains primarily more of the 2:17 phase and less α-Fe phase, which is almost entirely consumed in the subsequent peritectoid reaction. The optimal annealed $Nd_{14}Fe_{80}C_6$ alloy is dominated by 2:14:1 and 2:17 phases, thus the magnetic properties improved considerably.

Figures 4a and 5b–d show the same phase constitution in the partly crystallized and amorphous alloys after annealing. This indicates that the phase structure of the Nd-Fe-C alloy is not sensitive to the crystallization state of the alloy before annealing. However, in order to completely consume the α-Fe phase, the annealing temperature required for partly crystallized alloys is lower than that for amorphous alloys. This is due to the fact that some primary grains are already formed in partly crystallized alloys and less energy is required for the peritectoid reaction during annealing. In comparison, amorphous alloys require crystallization followed by a phase transformation, which requires higher energy. It should be noting that annealing at a lower annealing temperature may result in smaller grain size. Therefore, the partly crystallized annealed $Nd_{14}Fe_{80}C_6$ alloy exhibits better magnetic properties.

The optimal annealed alloy exhibits magnetic properties with J_r = 0.70 T, H_{cj} = 847 kA/m and $(BH)_{max}$ = 64 kJ/m^3 in this work, which are still lower than those of Nd-Fe-B annealed alloys. The melt spun Nd-Fe-B magnets were extensively studied. The melt-spun Nd-Fe-B alloys exhibit high magnetic properties with J_r up to 1.2 T, H_{cj} up to 1600 kA/m and $(BH)_{max}$ up to 190 kJ/m^3 [25–27]. In the reported work by previous researchers, the inferior properties of Nd-Fe-C alloys were attributed to the presence of the 2:17 phase. Coehoorn et al. [4] suggested that the 2:17 phase is more stable than the 2:14:1 phase due to the difference in carbon solubility. In this work, we found that the presence of the Nd_2O_3 phase and the undesirable microstructure are also responsible for the lower properties than Nd-Fe-B alloys. The large grain size up to 342 nm and the nonuniform grain size distribution in annealed $Nd_{14}Fe_{80}C_6$ alloy (Figure 7) are not beneficial to the hard magnetic properties. The grain size of the 2:14:1 phase in annealed Nd-Fe-B alloys is generally in the arrangement of 30 to 70 nm [28–30], which is finer and more uniform than that of Nd-Fe-C. In addition, the 2:17 phase with comparable grain size to 2:14:1 phase is presented in Nd-Fe-C alloys. Under an applied field, the magnetization reversal occurs preferentially in the 2:17 phase, leading to inconsistent demagnetization behavior. In addition, the Nd_2O_3 phase is distributed at triangular and quadrilateral grain boundaries reducing the magnetization and the remanence.

Based on the present results, in order to develop Nd-Fe-C magnets with high properties by making full use of the intrinsic magnetic properties of the $Nd_2Fe_{14}C$ compound, the soft magnetic 2:17 phase in the alloys should be suppressed. On the other hand, the grain size of the alloy should be further refined to obtain a higher coercivity. To achieve these goals, both the composition and the fabrication process of Nd-Fe-C magnets must be optimized. Most of all, more attention from academic and industrial fields should be paid to Nd-Fe-C alloys.

5. Conclusions

In this work, we revisited the phase structure, phase precipitation behavior and magnetic properties of the melt-spun ternary Nd-Fe-C alloys. A significant different phase precipitation behavior of the Nd-Fe-C system from Nd-Fe-B was manifested. As a result, the

excellent intrinsic magnetic properties of the $Nd_2Fe_{14}C$ compound cannot be fully utilized. It was confirmed that the hard magnetic $Nd_2Fe_{14}C$ phase cannot be formed directly by a rapid solidification of the liquid Nd-Fe-C alloy. The α-Fe phase in annealed alloys can be effectively eliminated by adjusting the composition of the alloy. For $Nd_{10+x}Fe_{80-x}C_6$ (x = −2, 0, 2, 3, 4, 5) annealed alloys, the content of the α-Fe phase decreases with increasing x and is almost eliminated when x = 3. The crystallization state of the Nd-Fe-C alloy before annealing has an effect on the optimum annealing temperature and the magnetic properties. The properties of the annealed amorphous $Nd_{14}Fe_{80}C_6$ alloy are J_r = 0.58 T, H_{cj} = 542 kA/m and $(BH)_{max}$ = 45 kJ/m^3, while those of the annealed partly crystallized $Nd_{14}Fe_{80}C_6$ alloy prepared at 20 m/s are J_r = 0.70 T, H_{cj} = 847 kA/m and $(BH)_{max}$ = 64 kJ/m^3. The optimal annealed alloy of $Nd_{14}Fe_{80}C_6$ consists of the 2:14:1 phase, 2:17 phase and Nd_2O_3 phase. To obtain better magnetic properties, further microstructure optimization may be carried out by suppressing the second phase and refining the grains.

Author Contributions: Conceptualization, Z.L. and H.Y.; methodology, Z.L., J.F. and B.Z.; validation, J.F. and B.Z.; formal analysis, J.F. and B.Z.; investigation, Z.L., H.Y., J.F. and B.Z.; resources, Z.L. and H.Y.; data curation, J.F.; writing—original draft preparation, J.F.; writing—review and editing, Z.L., J.F., H.Y. and B.Z.; visualization, J.F. and B.Z.; supervision, Z.L. and H.Y.; project administration, Z.L. and H.Y.; funding acquisition, Z.L. and H.Y. All authors have read and agreed to the published version of the manuscript.

Funding: This work is supported by the National Natural Science Foundation of China (No. U21A2052).

Data Availability Statement: The raw data supporting the conclusions of this article will be made available by the authors on request.

Conflicts of Interest: The authors declare no conflicts of interest.

References

1. Sagawa, M.; Fujimura, S.; Togawa, N.; Yamamoto, H.; Matsuura, Y. New material for permanent magnets on a base of Nd and Fe. *J. Appl. Phys.* **1984**, *55*, 2083–2087. [CrossRef]
2. Helmholdt, R.B.; Buschow, K.H.J. Neutron diffraction study of the crystallographic and magnetic structure of $Nd_2Fe_{14}C$. *J. Less-Common Mat.* **1988**, *144*, L33–L37. [CrossRef]
3. De Mooij, D.B.; Buschow, K.H.J. Formation and magnetic properties of the compounds $R_2Fe_{14}C$. *J. Less-Common Met.* **1988**, *142*, 349–357. [CrossRef]
4. Coehoorn, R.; Duchateau, J.P.W.B.; Denissen, C.J.M. Permanent magnetic materials based on $Nd_2Fe_{14}C$ prepared by melt spinning. *J. Appl. Phys.* **1989**, *65*, 704–709. [CrossRef]
5. Buschow, K.H.J.; De Mooij, D.B.; Denissen, C.J.M. Note on the formation and the magnetic properties of the compound $Nd_2Fe_{14}C$. *J. Less-Common Met.* **1988**, *141*, L15–L18. [CrossRef]
6. Van Mens, R. Ternary phase studies of Nd-Fe-X where X = C, Si, Ge, Pb, Sn. *J. Magn. Magn. Mater.* **1986**, *61*, 24–28. [CrossRef]
7. Denissen, C.J.M.; De Mooij, D.B.; Buschow, K.H.J. Spin reorientation in $Nd_2Fe_{14}C$. *J. Less-Common Mat.* **1988**, *142*, 195–202. [CrossRef]
8. Grieb, B.; Henig, E.-T.; Matinek, G.; Stadelmaier, H.H.; Petzow, G. Phase relations and magnetic properties of new phases in the Fe-Nd-Al and Fe-Nd-C systems and their influence on magnets. *IEEE Trans. Magn.* **1990**, *26*, 1367–1369. [CrossRef]
9. Grieb, B.; Fritz, K.; Henig, E.-T. As-cast magnets based on Fe-Nd-C. *J. Appl. Phys.* **1991**, *10*, 6447–6449. [CrossRef]
10. Fernengel, W. Microstructure and magnetic properties of sintered Nd-Fe-C magnets. *IEEE Trans. Magn.* **1994**, *30*, 634–635. [CrossRef]
11. Sui, Y.C.; Zhang, Z.D.; Xiao, Q.F.; Liu, W.; Zhao, X.G.; Zhao, T.; Chuang, Y.C. Nd–Fe–(C, B) permanent magnets made by mechanical alloying and subsequent annealing. *J. Phys.-Condens. Mat.* **1996**, *8*, 11231–11242. [CrossRef]
12. Sui, Y.C.; Zhang, Z.D.; Liu, W.; Xiao, Q.F.; Zhao, X.G.; Zhao, T.; Chuang, Y.C. Mechanically alloyed isotropic (Nd,Dy)-Fe-C magnets. *J. Magn. Magn. Mater.* **1997**, *170*, L17–L21. [CrossRef]
13. Sui, Y.C.; Zhang, Z.D.; Xiao, Q.F.; Liu, W.; Zhao, T.; Zhao, X.G.; Chuang, Y.C. Structure, phase transformation and magnetic properties of Nd-Fe-C alloys made by mechanical alloying and subsequent annealing. *J. Alloys Compd.* **1998**, *267*, 215–223. [CrossRef]
14. Hayashi, N.; Daniil, M.; Zhang, Y.; Hadjipanayis, G.C. Structural and magnetic properties of Nd-(Fe,M)-(C,B) melt-spun ribbons. *J. Alloys Compd.* **2000**, *305*, 290–297. [CrossRef]
15. Geng, H.M.; Ji, Y.; Zhang, J.J.; Gao, Y.C.; Yan, Y.; Wang, W.Q.; Su, F.; Du, X.B. $Nd_2Fe_{14}C$-based magnet with better permanent magnetic properties prepared by a simple mechanochemical method. *J. Magn. Magn. Mater.* **2017**, *441*, 209–216. [CrossRef]

16. Yang, J.B.; Gutfleisch, O.; Handstein, A.; Eckert, D.; Müller, K.H. High coercivity of Nd-Dy-Fe-(C,B) ribbons prepared by melt spinning. *Appl. Phys. Lett.* **2000**, *76*, 3627–3629. [CrossRef]
17. Yang, J.B.; Handstein, A.; Kirchner, A.; Gutfleisch, O.; Müller, K.H. Magnetic properties of melt-spun $(Nd,Dy)_2Fe_{14}(B,C)$. *J. Alloys Compd.* **2001**, *316*, 290–295. [CrossRef]
18. Vystavkina, V.; Brekharya, G.; Vasil'yeva, E.; Leonowicz, M. Magnetic properties and microstructure of Nd-Fe-B-C magnets with Cu addition. *J. Magn. Magn. Mater.* **2004**, *284*, 69–76. [CrossRef]
19. Zhang, W.Y.; Zhang, J.; Zhang, S.Y.; Shen, B.G. High coercivity $Nd_2(Fe,Co)_{14}C$-type ribbons prepared by melt spinning. *J. Magn. Magn. Mater.* **2001**, *234*, 284–288. [CrossRef]
20. Tu, H.R.; Yan, Y.; Cai, D.; Wang, J.X.; Shang, X.Y.; Tian, H.; Su, F.; Du, X.B. Effects of solvent and annealing on phase evolutions and magnetic properties of $Nd_2(Fe,Co)_{14}C$ hard magnetic powders prepared by mechanochemical method. *Mater. Des.* **2019**, *183*, 108140. [CrossRef]
21. Liu, Z.W.; He, J.Y.; Zhou, Q.; Huang, Y.L.; Jiang, Q.Z. Development of non-rare earth grain boundary modification techniques for Nd-Fe-B permanent magnets. *J. Mater. Sci. Technol.* **2022**, *98*, 51–61. [CrossRef]
22. He, J.Y.; Zhou, B.; Liao, X.F.; Liu, Z.W. Nanocrystalline alternative rare earth-iron-boron permanent magnets without Nd, Pr, Tb and Dy: A review. *J. Mater. Res. Technol.* **2024**, *28*, 2535–2551. [CrossRef]
23. Wang, L.; Wang, J.; Rong, M.H.; Rao, G.H.; Zhou, H.Y. Effect of wheel speed on phase formation and magnetic properties of $(Nd_{0.4}La_{0.6})$-Fe-B melt-spun ribbons. *J. Rare Earths* **2018**, *36*, 1179–1183. [CrossRef]
24. Schneider, G.; Henig, E.-T.; Petzow, G.; Stadelmaier, H.H. Phase relations in the system Fe-Nd-B. *Int. J. Mater. Res.* **1986**, *77*, 755–761. [CrossRef]
25. Poenaru, I.; Patroi, E.A.; Patroi, D.; Iorga, A.; Manta, E. HDDR as advanced processing method and recycling technology to address the rare-earth resource criticality in high performance $Nd_2Fe_{14}B$. *J. Magn. Magn. Mater.* **2023**, *577*, 170777. [CrossRef]
26. Hütten, A.; Thomas, G. Microstructural parameters of melt-spun $Nd_{15}Fe_{77}B_8$ ribbons. *Ultramicroscopy* **1992**, *47*, 447–454. [CrossRef]
27. Zeng, X.R.; Sheng, H.S.; Jin, C.J.; Qian, H.X. Magnetic properties and microstructure of melt-spun $Nd_2Fe_{14}B/\alpha$-Fe nanocomposite magnets with a perpendicular anisotropy. *J. Magn. Magn. Mater.* **2016**, *401*, 1155–1158. [CrossRef]
28. Mishra, R.K. Microstructure of melt-spun Nd-Fe-B magnequench magnets. *J. Magn. Magn. Mater.* **1986**, *54*, 450–456. [CrossRef]
29. Hashino, H.; Tazaki, Y.; Ino, H.; Ohkubo, T. Effects of Zr and C additions on the magnetic properties and structures of melt-spun $Fe_{83}Nd_{10}B_7$-based nanocomposite magnets. *J. Magn. Magn. Mater.* **2004**, *278*, 68–75. [CrossRef]
30. Pei, K.; Zhang, X.; Lin, M.; Yan, A. Effects of Ce-substitution on magnetic properties and microstructure of Nd–Pr–Fe–B melt-spun powders. *J. Magn. Magn. Mater.* **2016**, *398*, 96–100. [CrossRef]